Taylor & Francis
Taylor & Francis Group

Check for updates

3D Boundary element meshing for multiscale bone anisotropic analysis

D. M. Prada, A. F. Galvis ![ORCID], A. C. Alcântara and P. Sollero

Department of Computational Mechanics, School of Mechanical Engineering, University of Campinas, Campinas, Brazil

ABSTRACT

Bone health conditions are treated with prosthesis and implant fixations. Despite being there to assist the patient, the difference between the elastic properties of these artificial medical solutions and the treated bone region may lead to a new fracture. One strategy to circumvent that problem, reducing the gap between the elastic properties, is to use Functionally Graded Materials in the manufacture of such medical devices. It is therefore of vital importance to understand the mechanical properties of bone within the region of interest, once this knowledge may ease and improve the development of artificial medical solutions. The bone tissue is a hierarchical material which has different elastic behaviour depending upon the scale of interest, the particular bone and the bone region. In this work, a multi-scale BEM mesh model of bone tissue ranging from the nanoscale to the mesoscale is sought. A new nanoscale design which considers the hydroxyapatite crystals inside, and outside the fibrils is developed. Furthermore, the fibrils are modelled with reported elliptical cross sections. Additionally, a procedure to develop the BEM meshes using multimedia software is proposed, based upon the similarities between them. Finally, several mesheswere created using triangular continuous elements.

1. Introduction

Many health conditions are related with bone tissue. While some of them are due to traumatic injuries, others are a consequence of bone infections or degenerative diseases. When these conditions come to a fracture, the treatment commonly involves an internal fixation in order to accelerate the bone healing process. Additionally, there are other situations where a correct bone alignment or replacement using specialized devices and implants is needed. In general, when the patient's health condition is favourable, the treatment chances of success are relatively high. However, in the presence of risk factors, the previous procedures could be a cause of further fractures due

---

to stress shield (Reiser, Hricak, & Knauth, 2013). This mechanical phenomenon occurs because of the difference between the effective elastic constant's values of the bone and the implant's biomaterial. Aiming to overcome this problem, a few strategies have been proposed as for example, the use of porous and functionally graded biomaterials (He, Zhan, Jiang, & Zhou, 2017; Ryan, Pandit, & Apatsidis, 2006; Shirazia, Ayatollahia, & Asnafib, 2017). Nevertheless, to successfully implement these strategies, it is necessary to know the elastic properties of the bone.

Human bones are classified under four groups: long, short, flat and irregular bones. They perform seven important functions: support, protection, mineral and growth factor storage, blood cell formation, triglyceride storage and hormone production (Sabet, Najafi, Hamed, & Jasiuk, 2016). Bone is a complex tissue which is organized as follows: (1) the macroscale: this scale represents the whole bone; (2) the mesoscale (up to a few millimetres): trabecular and cortical bone; (3) the microscale (up to 500 μm): Harvesian systems, osteons, single trabecula; (4) the sub-microscale (up to 20 μm): lamella; (5) the nanoscale (up to 1000 nm): mineralized fibrils embed in a matrix of hydroxyapatite crystals (HA) and water; (6) sub-nanoscale (up to 50 nm): HA and collagen microfibrils; and (7) molecular scale: molecular structure of constituent elements (Rho, Kuhn-Spearing, & Zioupos, 1998; Sabet et al., 2016). The hierarchical bone structure is widely known. However, the nanoscale and sub-nanoscale morphology have been a recent discussion issue. In this work these scales were modelled as it is shown in Figure 1.

Numerous multi-scale bone structure models have been proposed in the literature. In (Vaughan, McCarthyb, & McNamaraa, 2012), bone is modelled at the nanostructural level as a composite, whose matrix consists of HA (matured mineral) distributed within collagen. Other authors, subdivided the nanoscale in microfibrils, fibrils and fibres, distributing the HA among the subdivisions (Barkaoui, Tlili, & Vercher-Martnez, 2016). Barkaoui, Chamekh, Merzouki, Hambli, and Mkaddem (2014),use the model developed in (Barkaoui et al., 2016) to obtain the elastic constants of the cortical bone considering the presence of water within the minor scales. All these models represent the fibrils as cylinders with circular cross section.

In this work, the nanoscale structure of bone is modelled as fibrils with elliptical cross section, as it was reported in (McNally, Schwarcz, Botton, & Arsenault, 2012). Furthermore, water, as a constituent of the nanoscale, is considered within collagen, HA and HA-collagen composites. The implementation of the mineral into the model was made such that, 20% of the mineral distribution can be found inside the fibrils and the remaining 80% lies outside the fibrils. A new strategy is developed in the trabecular bone, where each trabecula is regarded as a region with a proper elasticity tensor and anisotropic direction. For the first time, a 3D BEM formulation is applied for the analysis of the described anisotropic bone hierarchical structure. The aim of this work
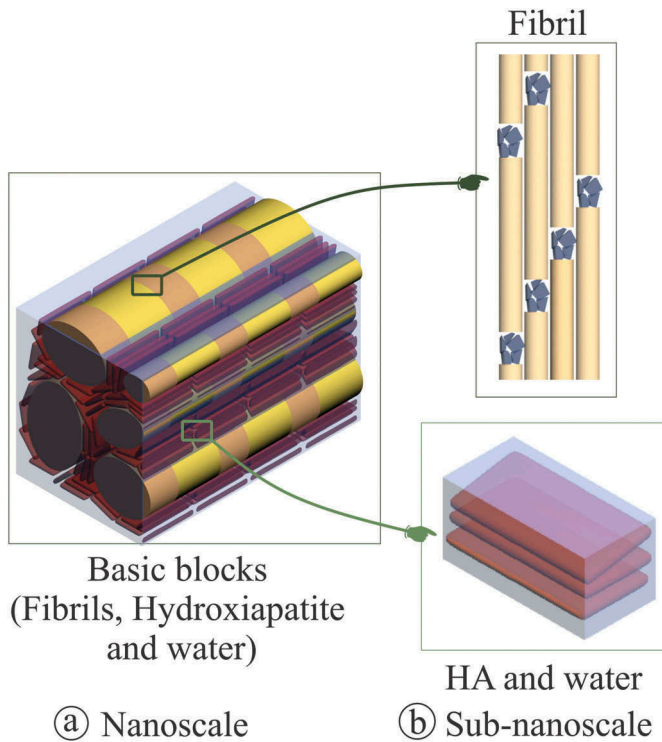
Figure 1. (a) Nanoscale: Fibrils embed on the matrix. (b) Sub-nanoscale: HA and microfibrils (Ritchie, Buehler, & Hansma, 2009).

is however to define and model the meshes of the multi-scale analysis. It is important to highlight that BEM could simplify the bone remodelling process. This work has been conducted thinking in future applications of BEM in anisotropic bone remodelling. Surface meshes are required for carrying out the BEM analysis. The big majority of the mesh generators are volumetric, turning the discretization of complex surface models into a hard task. Hence, a technique is proposed using a multimedia software. The generated meshes are illustrated and described for the multi-scale analysis.

2. Hierarchical bone structure model

2.1. Macroscale: whole bone

The major scale of the hierarchical structure is the whole bone (Podshivalov, Fischer,& Bar-Yoseph, 2014). It represents any bone in its entirety. One way to model the bone morphology is through a Computerized Tomography (*CT*), which allows the determination of the cortical and the trabecular region. Additionally, it is possible to use *CT*s in conjunction with bone densitometries in order to improve the resolution of the model in development.

2.2. Mesoscale: trabecular bone

A step forward to zooming in, the whole bone is divided into two categories. The trabecular bone's main mechanical function is to absorb the energy of impact loads, and the cortical bone gives the stiffness and mechanical strength to bones. As shown in Figure 2, the trabecular bone consists basically of a three-dimensional rope net structure immersed within bone marrow, just as a scaffold in a pool. This tissue can be parameterized using: trabecular bone thickness ($TbTh$), it means the thickness of the rods; average trabecular bone separation ($TbSp$), basically the separation between rods, and percentage bone volume (bone volume [BV]/total volume [TV]) (Hsu et al., 2013) In this work, the parameters were set as $TbTh = 0.1$ mm, $TbSp = 0.37$ mm and $BV/TV = 13.98\%$ (Muller et al., 1998)

In order to assess the elastic properties of trabecular bone, it is needed to take into account that each trabecula has an anisotropic behaviour, which is represented by the stiffness tensor determined within a coordinate system. For instance, in Figure 2, it is possible to see, in a magnified view, the trabeculas $T1$, $T2$ and $T3$ and its respective z-directions Z'_{T1}, Z'_{T2} and Z'_{T3}. In the representative volume element (RVE) of trabecular bone, the stiffness tensor of each trabecula must be kept on its local coordinate system. To solve this issue, the RVE was hereby divided into multiple subdomains, each having its own coordinate system (the local coordinate system). This solution uses an approximate z-direction, which is easy to get for trabeculas but is not that straightforward for the nodes. To obtain the z-direction of the nodes, a normalized vector (Z'_N) is evaluated using the normal of each interface belonging to the interest node. It is important to highlight that,
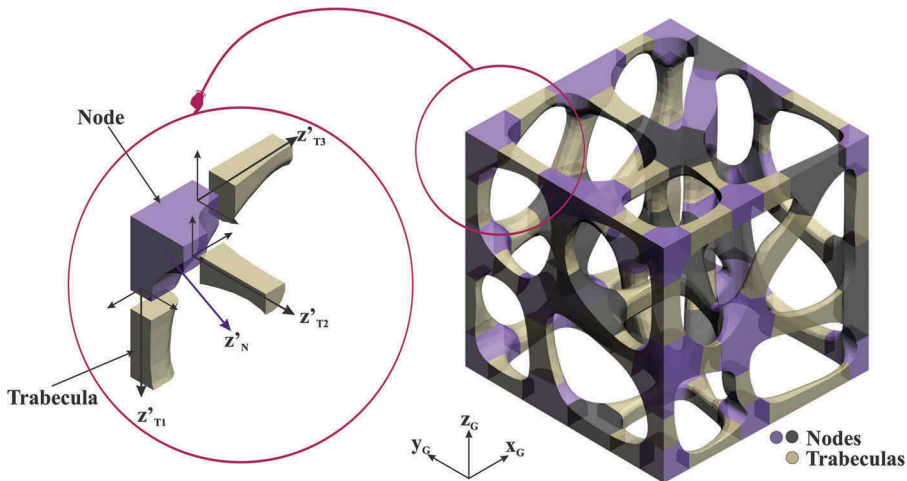

Figure 2. Representative Volume Element (RVE = 1 mm × 1 mm × 1 mm) of the trabecular bone using $TbTh = 0.1$ mm, $TbSp = 0.37$ mm, $BV/TV = 13.98\%$.

in the case shown in Figure 2, the interface normals are the same as trabecula z-axis. However, this is not always true and care must be taken to avoid mistakes.

2.3. Mesoscale: cortical bone

A Haversian system is basically lamellae arranged around a Haversian canal forming a body which resembles a cylinder, also called osteon. Finally, the cortical bone is composed by an arrangement of parallel osteons and leftovers of themselves (Rho et al., 1998). The precise geometrical form of osteons depends on many factors. However, within this research, the osteons and Haversian canals were assumed cylinders and holes (Vaughan et al., 2012). Figure 3 shows the RVE of the cortical bone using such assumptions. Cortical bone tissue can be described by its thickness and by the canal volume fraction or cortical bone porosity Ca. V/Total.V (Dong et al., 2014) set as 0.006.

2.4. Microscale: trabecula and osteon

As we mentioned above, the trabecular bone is basically a net of rods. Therefore, the microscale is a single rod (trabecula). Inside the cortical tissue, the microscale represents the isolated Harversian system. For mechanical purposes, these structures just differ on a trabecula does not have a Harversian canal. Then, the microstructure is the same for both tissues, and it is a concentric arrangement of cylindrical layers called lamellae. Additionally, as is described on the next subsection, lamellae are composed by fibrils, which are oriented in such a way that they have an inclination with respect to its osteon axis. The RVE of the sub-microscale is shown in Figure 4.
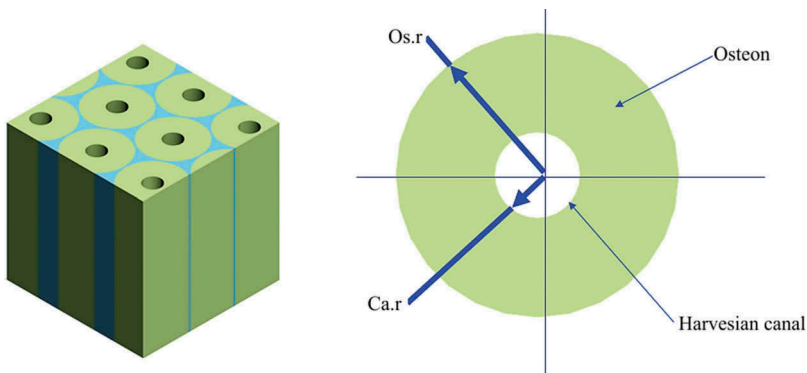

Figure 3. RVE (1 mm × 1 mm × 1 mm) of the cortical bone. The osteon radius (Os.r) and the canal radius (Ca.r) were set as 100μm and 30μm, respectively. These parameters are in accordance with the aforementioned Ca.V/Total.V = 0.006.
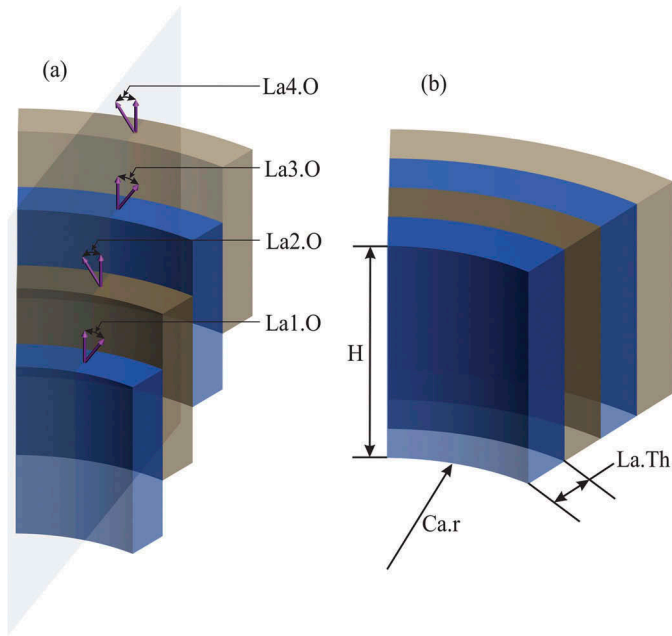
Figure 4. (a)Exploded view of the sub-microscale with emphasis on the orientation of the lamellae ($La1.O/La1.O/La1.O/La1.O = 15°/-15°/15°/-15°$); (b) RVE of the sub-micro-scale and its parameters. Height ($H = 60\,\mu mm$), canal radius ($Ca.r = 30\,\mu m$) and lamella thickness ($La.Th = 60\,\mu m$).

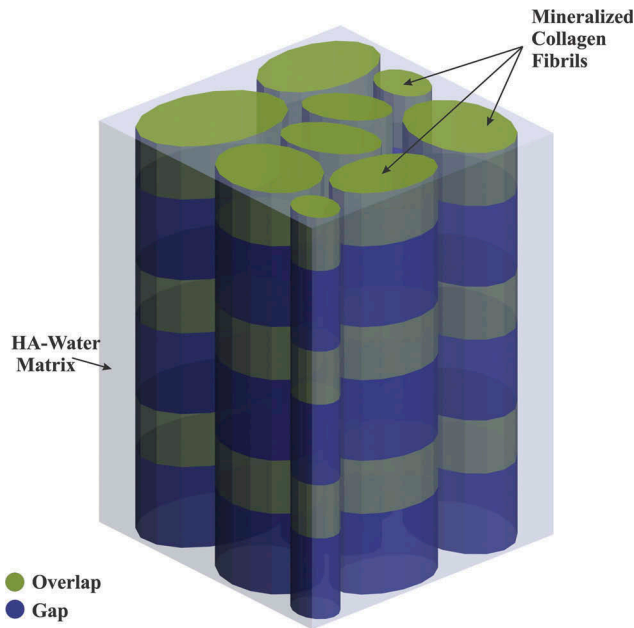**Figure 5.** RVE ($164\,mm \times 164\,mm \times 204\,mm$) of the nanoscale using nine elliptical cross section fibrils, MVF = 40% and a water content of 20%.

2.5. Nanoscale: basic blocks

A little further on, it is reached the nanoscale. This is described by an arrangement of fibrils embedded in a matrix of HA and water, as it is shown in Figure 1(a). The dimensions of HA crystals have been a matter of discussion. Early studies using Transmission Electron Microscopy (TEM) and X-Ray have reported 40 60 nm in length, 20 30 nm in width and 1.5 4 nm in thickness. Using Atomic Force Microscopy (AFM) techniques, Sabet et al. (2016) have been reported larger dimensions, approximately 30~200 nm. Recently, through Dark-Field Electron Microscopy (DF), it was found that the length is 10 100 nm, the width has a few tens of nm and thickness is 5 6 nm (Schwarcz, McNally, & Botton, 2014). The distribution of the HA crystals in the nanoscale is not fully understood. However, there are recent studies that show that 80% of the mineral in the form of HA crystals lies outside the collagenfibrils. As it is shown in the Figure 5, this scale was modelled as acomposite material, where the matrix is made of HA crystals and water, and the inclusions are mineralized collagen fibrils (Nair, Gautieri, & Buehler, 2014; Sabet et al., 2016; Vaughan et al., 2012). It is worth highlighting that the other 20% remains inside the collagen fibrils, and it has to be considered in any mechanical analysis. Mineralized collagen fibrils are cross-linked collagen molecules, HA and water (Hamed & Jasiuk, 2012). Another important issue is the Mineral Volume Fraction (MVF) which means the percentage of mineral into a unit volume (Ghanbari & Naghdabadi, 2009; Vaughan et al., 2012). Its value commonly is between 32 and 52% (Barkaoui et al., 2016)

Here, the nanoscale was modelled by setting MVF on 40% and taking into account that 80% of HA remains into the matrix. As it was said before, the matrix is composed by HA and water. However, it is modelled as a single material, and its effective elastic properties can be evaluated using the Voigt and Reuss bonds for composites (Yoon & Cowin, 2008). Mineralized collagen fibrils are composed by water, HA, collagen with a morphology close to cylindrical shape with elliptic cross section, in which the major and minor axes have a length of 54.6 ± 23.9 nm and 36.3 ± 18.1 nm respectively (McNally et al., 2012). Additionally, in the longitudinal direction, fibrils have a periodic structure divided in two parts. The first one is called the overlap. It represents a 40% of the period D and contains only water and collagen. The last one is called the gap. It represents a 60% of period D, and in it resides the 20% interfibrilar HA (Barkaoui et al., 2016; Schwarcz et al., 2014). In this work, the fibrils were modelled as a cylinder with the previously mentioned elliptical cross-sections. Each cylinder has a periodic structure with a period D = 67 nm (Barkaoui et al., 2016). The overlap and gap zones as well as the matrix are modelled as a homogeneous material. The effective elastic properties can be

determined by Voigt and Reuss bounds. Finally, the water content was set as 20% and it was divided into two equal parts, one for the matrix and the other for the fibrils (Barkaoui et al., 2016).

3. Three-dimensional boundary element mesh

The boundary element method (BEM) has the ability to model high gradients of different mechanical fields only using the surface area information. The surface discretization leads to a reduction in the number of degrees of freedom (DOFs) used in the model. Depending on the application, a specific fundamental solution is required by the boundary integral equation. In this work, the displacement fundamental solution based on double Fourier's series, recently proposed by Tan, Shiah, and Wang (2013), will be used. Efficient schemes to evaluate the fundamental solution and the Green's functions is presented in detail in Shiah, Tan, and Wang (2012a, 2012b)) In case of different constitutive domains, the multi-domain algorithm (Galvis, Rodriguez, Sollero, & Alburquerque, 2013; Kane, 1994) needs to be implemented for some bone scales. Furthermore, Dirichlet and Neumann boundary conditions can be applied in the model.

3.1. Integral formulation

The boundary integral equation expresses the relationship between displacement u_i and traction t_i responses on a surface G using a known fundamental U_{ik} and T_{ik} state. For a homogeneous elastic body, the integral equation in absence of body forces, is given by

$$c_{ik}(X')u_i(X') + \int_G T_{ik}(X',X)u_i(X')\,\mathrm{d}\Gamma = \int_G U_{ik}(X',X)t_i(X')\,\mathrm{d}\Gamma \quad, \quad (1)$$

where (X') and (X) are the source and field points, respectively; $c_{ik}(X')$ is $\delta_{ik}/2$ to a smooth surface boundary at the source point; $U_{ik}(X',X)$ and $T_{ik}(X',X)$ are the fundamental solutions of displacement and traction, respectively. In a discretized form, Equation (1) is expressed by

$$c_{ik}(X')u_i(X') + \sum_{j=1}^{N_{el}} \int_G T_{ik}(X',X)u_i(X)\,\mathrm{d}\Gamma = \sum_{j=1}^{N_{el}} \int_G U_{ik}(X',X)t_i(X)\,\mathrm{d}\Gamma \quad,$$

$$(2)$$

where, N_{el} is the number of elements. In matrix form, the Equation (2) becomes

$$\mathbf{Hu} = \mathbf{Gt}, \quad (3)$$

where **H** and **G** are the matrices from the integration of the traction T_{ik} and displacement U_{ik} fundamental solution, respectively. The integration is carried out among the source points (*sp*), source elements (*se*) and field elements (*fe*). Singular and regular integration schemes for triangular and quadrilateral continuous or discontinuous elements can be found in more detail in Aliabadi (2002) and Kane (1994).

3.2. Multi-domain algorithm

Solids composed by different domains are modelled by the multi-domain algorithm. It is recommended that the implementation of this algorithm is by using discontinuous boundary elements, to avoid nodes shared by more than two domains. This fact helps the implementation, despite the number of the DOFs is increased with discontinuous elements. Figure 6 shows an interface between two domains Ω_i and Ω_j. Γ_i and Γ_j are the interface surfaces, and $\bar{\mathbf{n}}$ is the outward normal vector. In this case, three-node discontinuous triangular boundary elements el_i and el_j are also shown, where the total compatibility is required between the physical *Pn* and geometrical *Gn* nodes from the mesh generation.

Here, in order to establish the final system of equations, a displacement compatibility $\mathbf{u}_i^j = \mathbf{u}_j^i$ and traction $\mathbf{t}_i^j = -\mathbf{t}_j^i$ equilibrium in the interfaces between *i*th and *j*th domains must be applied. For this illustrative case, the final system of equation after the application of the boundary conditions is given by

$$\begin{bmatrix} \mathbf{A}_i & \mathbf{H}_i^j & -\mathbf{G}_i^j & 0 \\ 0 & \mathbf{H}_j^i & \mathbf{G}_j^i & \mathbf{A}_j \end{bmatrix} \begin{Bmatrix} \mathbf{X}_i \\ \mathbf{u}_i^j \\ \mathbf{t}_i^j \\ \mathbf{X}_j \end{Bmatrix} = \begin{bmatrix} \mathbf{B}_i & 0 & 0 & 0 \\ 0 & 0 & 0 & \mathbf{B}_j \end{bmatrix} \begin{Bmatrix} \mathbf{k}_i^{bc} \\ 0 \\ 0 \\ \mathbf{k}_j^{bc} \end{Bmatrix} , \quad (4)$$
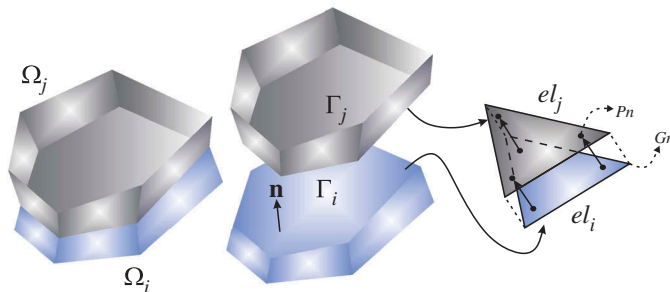

Figure 6. Interface between two domains.

where $\mathbf{A}_i$ and $\mathbf{B}_i$ are the blocks corresponding to $\mathbf{H}_i$ and $\mathbf{G}_i$ that belong to the boundary of the overall domain where the load conditions are applied. The blocks $\mathbf{H}_i^j$ and $\mathbf{G}_i^j$ correspond to the interfaces between ith and jth domains. Vector $\mathbf{X}_i$ contains all the traction and displacement unknowns to be evaluated in the elements that correspond to the boundaries of the overall domain, $\mathbf{k}_i^{bc}$ refers to the known boundary conditions. Displacement $\mathbf{u}_i^j$ and traction $\mathbf{t}_i^j$ are calculated in the interfaces. The final three block matrices and vector in Equation (4) for this application are highly sparse due to the incidence between the domains. Thus, in order to improve the implementation in terms of RAM memory and computational processing it is needed to treat all operations between these systems as a sparse. The final matrix equation is

$$\mathbf{Ax} = \mathbf{Bk}^{bc} \quad . \tag{5}$$

3.3. Homogenization properties

Several applications in engineering require detailed analysis of material behaviour throughout different scales of space and time. Additional physical effects are considered using a microscale material modelling, such as the anisotropic constitutive behaviour, flaws, stochastic morphology and defects. It is useful in the multi-scale analysis, the evaluation of the macroscopic constitutive behaviour of the material points using the information of the heterogeneities in the microscale (Zohdi & Wriggers, 2005). The average homogenization (Hill, 1963) can be used to this end. Taking advantages of the features of the BEM, it is possible to obtain a homogenized stress tensor of the microscale using the direct displacement and traction field evaluated by the BEM, Equation (6)

$$\langle \hat{\sigma}_{ij} \rangle = \frac{1}{|\Omega|} \int_{\Omega} \sigma_{ij} \, d\Omega = \frac{1}{2|\Omega|} \int_{\Gamma} \left(t_i x_j + t_j x_i \right) d\Gamma \tag{6}$$

and for the strain field gives

$$\langle \hat{\varepsilon}_{ij} \rangle = \frac{1}{|\Omega|} \int_{\Omega} \varepsilon_{ij} \, d\Omega = \frac{1}{2|\Omega|} \int_{\Gamma} \left(n_i u_j + n_j u_i \right) d\Gamma \quad . \tag{7}$$

In Equations (6) and (7) $|\Omega|$ is the volume of the representative element, u_i and t_i are the displacement and traction responses, respectively. Applying the Hooke's law using the homogenized tensors in Equations (6) and (7) gives

$$\langle \bar{\sigma} \rangle = \bar{\mathbf{C}} : \langle \bar{\varepsilon} \rangle \tag{8}$$

where $\bar{\mathbf{C}}$ is the apparent elasticity tensor that characterizes the macroscopic constitutive behaviour of the microscale. In order to evaluate all the 36 components of $\bar{\mathbf{C}}$, a set of six independent kinematic boundary

conditions can be applied (Benedetti & Aliabadi, 2013; Fritzen, Hlke, & Schnack, 2009). Some materials present random geometrical and constitutive configuration, making necessary a statistic analysis to obtain a good confidence interval in the numerical results of the apparent elastic properties.

3.4. Computational aspects

The BEM, usually implemented in Fortran or C++, can be optimized using the Message Passage Interface (MPI) on a distributed memory architecture to obtain more computational efficiency in terms of memory and processing time. Therefore, it is required to parallelize the critical sections in the overall algorithm, such as the determination of the interfaces, see Figure 6. The computation of the matrices **H** and **G** in Equation (3) is done with an adequate balance distribution data between the processors. For the solution of the final system of Equation (5), a Multi-frontal Massively Parallel Sparse (MUMPS) direct solver (Amestoy, Duff, Koster, & L'Excellent, 2001; Amestoy, Guermouche, L'Excellent, & Pralet, 2006) is recommended and available in http://mumps.enseeiht.fr/. MUMPS implements a direct method based on a multi-frontal approach which performs a Gaussian factorization.

4. Meshing process using multimedia software

On the multimedia design and game development field, there are a lot of specialized software which make the modelling and discretization work easier. In particular, this kind of software works like CAD software. But instead of build bodies, it builds superficial meshes and it assigns, to each element, visual properties like colours and illumination patterns. This field has been constantly improving since its creation, circa 90s. Therefore, there are quite a few robust softwares available up to date.

In this work, it was established a procedure to use Autodesk 3ds Max (a multimedia software) to meshing BEM models. However, this procedure could be adapted to use another multimedia software, like blender or Autodesk Maya. Many multimedia softwares are available on the market and any of those can be used. In this work, It was selected Autodesk 3ds Max. Due to, for the best of our knowledge, it is the most used multimedia software. Then, it has more support for its community than the others. Additionally, Autodesk provides the full version for free, for academic purposes.

Firstly, a primitive geometry is created using the Primitives menu, which is a surface since its creation. After that, through Modifiers menu, the geometry has to be modified until it gets the wanted shape. For BEM, the most useful Modifiers' tools are Edit poly and Edit mesh, which allows

to manually modify the elements and vertices; Quadify, which turns the default triangular mesh into a quadrilateral one; Subdivide, which set the maximum length parameter of every element in the mesh; Optimize, it generates a new mesh using the minimum possible elements for a given geometry and finally Relax, which reduce the apparent surface tension. When a multi-domain model is considered, the next step is to guarantee the consistency of the model interface. This means that if two interfaces are in contact, both have to be meshed with the same elements in order to couple the domains during the BEM process. For this task, the software, using the Clone tool, allows to clone an interface of one domain to subsequently attach it to another domain. Another BEM model issue is the normal of each element. They can be seen and edited using the options See Normals and Flip, into the Edit Mesh modifier. Finally, the export process is made by selecting the .obj format. It is a list with the coordinates of the vertices and the concatenation of such vertices which form the elements. In the text, the word 'Object' means a new domain; the letter 'v' means that the textline contains vertices coordinates and the letter 'f' means that the textline contains an element. The numbering of domains, vertices and elements are sequential. The normals have to be calculated with the cross product between the vectors conformed by the vertices of each element.

5. Results and discussion

In this section, the meshing process results are presented. Figure 7 shows the meshes for the nanoscale, trabecula and osteon and cortical bone. Through the mentioned meshing process, the compatibility between elements of different regions is guaranteed. Also, an adequate distribution of the size of the triangular elements, as shown in Figure 7(a,b), is required to avoid errors in the numerical integration of the BEM formulation. The meshes were generated using triangular continuous elements. However, they are converted to discontinuous elements using shape functions in a Fortran code.

In general, some basic information to analyse these physical models is required, such as the number of regions, number of elements, compatibility matrix for elements, the Cartesian coordinates of each node and the outward normal vectors for each element. For more details of the implementation and input data requirements, see Galvis, Rodriguez, & Sollero, (2018).

In Figure 8, the trabecular bone is presented. This mesh represents a difficult challenge to be generated owing to the irregular character of the approximate surface curves by flat elements. However, as illustrated in Figure 8, the final results in terms of mesh density and size elements are adequate for BEM analysis.
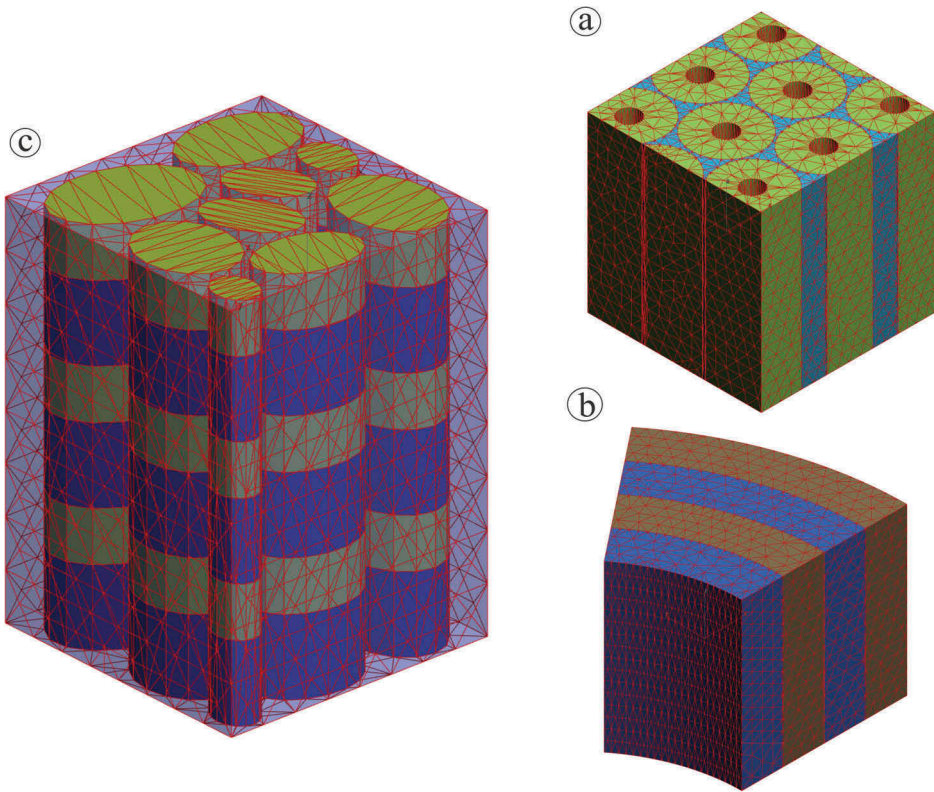
Figure 7. Superficial meshes of: (a) cortical bone; (b) trabecula and osteon; (c) nanoscale.
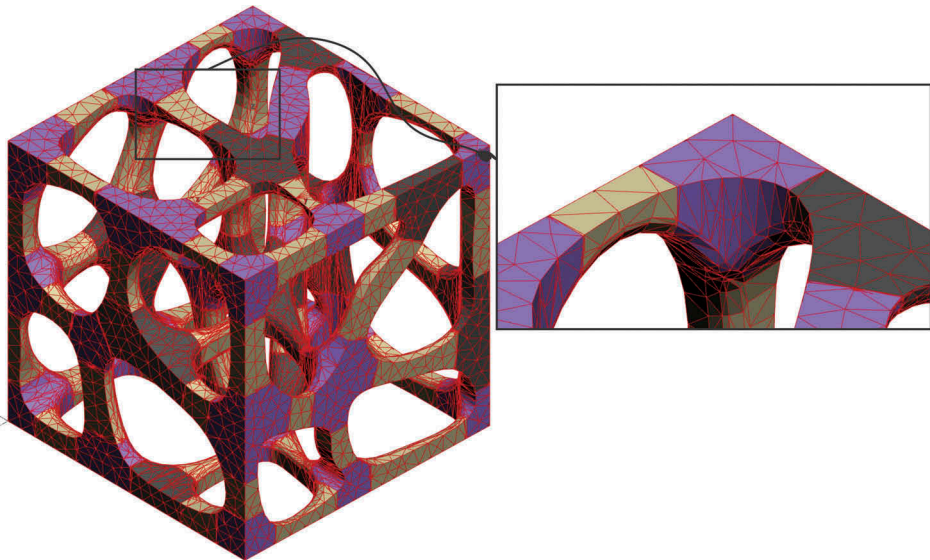

Figure 8. Superficial mesh of the trabecular bone.

Table 1. Number of elements and DOFs of the generated bone multi-scale BEM models.

	Trabecular bone	Cortical bone	Trebecula and osteon	Nanoscale
Elements	32,618	40,734	9438	6387
DOFs	293,562	366,606	84,942	57,483
Subdomains	84	11	4	55

The number of elements and the DOFs of each scale are presented in Table 1. The distributions of the elements are largely dependent on the way which the solids are made.

The base solid to generate the meshes *a*, *b*, and *c* in Figure 7, were directly modelled using *Autodesk 3ds Max*. The base solid used to generate the mesh in Figure 8 was modelled using *Autodesk Inventor* and it was exported on .stl format to *Autodesk 3ds Max*. As it can be seen in Figure 8, the mesh is not as homogenous as it was desired. Nevertheless, results are sufficiently good to be implemented in BEM. As mentioned before, the scope of this paper is the definition and modelling of the different multi-scale meshes. For future remarks, the multi-scale approach will be described here. In Section 3, it was pointed out the formulation and numerical implementation aspects of the 3D BEM, also the homogenization process adapted to the BEM was described.

5.1. Multi-scale modelling

The multi-scale approach begins by the definition of the basic constituents, which are water, Ha and collagen. Each one of these has known elastic properties represent by the tensors $\mathbf{C}_w$, $\mathbf{C}_{HA}$ and $\mathbf{C}_c$, respectively. The sub-nanoscale is formed by three composite materials. In Figure 7(c), the 'green' material is a composite of water and collagen. The 'blue' material is a composite of water, collagen and HA. Finally, the matrix is a composite of water and HA. The tensor of elastic properties of the composite materials for the sub-nanoscale could be obtained using the Voigh and Reuss bounds (Yoon & Cowin, 2008). Now, the nanoscale homogenized elastic properties $\langle \mathbf{C} \rangle_{nano}$ could be evaluated using the Equations 6, 7 and 9.

The following scale is the microscale, Figure 7(b). This scale has a cylindrical anisotropy. However, the difference between the RVE's length of the nanoscale and microscale allows to assume that the elastic properties $\langle \mathbf{C} \rangle_{nano}$ for an infinitesimal material point, represented in Cartesian coordinates, correspond to a local elastic properties directly in cylindrical coordinates $\langle \mathbf{C} \rangle_{micro}^{L}$. In the microscale, the fibrils inside the lamellae have an inclination with respect to the axial axis. Figure 7(b) shows this scale is composed by four regions (lamellae). In the 'blue' regions the tensor $\langle \mathbf{C} \rangle_{micro}^{L}$ is rotated 15° clockwise from the *z*-axis and the 'gray' region 15 counter-clock wise both on the *z*-θ plane. This stages requires

a cylindrical homogenization as proposed in (Sun et al., 2014). The result of this homogenization is the macroscopic elastic tensor in Cartesian coordinates for the trabecula and osteon material $\langle \mathbf{C} \rangle_{micro}$.

The fourth scale is the cortical bone, Figure 7(a). This scale is composed by two regions, the cylinders or 'green' regions are modelled using the $\langle \mathbf{C} \rangle_{micro}$ directly from the last scale. For the matrix or 'blue' region, it is proposed to use a tensor properties resulting from a previous homogenization of flat lamellae. The overall homogenization of the cortical bone is carried out applying again the Equations 6, 7 and 9 producing a new tensor $\langle \mathbf{C} \rangle_{cb}$. Finally, the trabecular bone shown in Figure 8 could be analysed using the tensor $\langle \mathbf{C} \rangle_{micro}$. due to the microscale is also the constitutive material of trabecular bone. As it is shown in Figure 2, the trabecular bone is composed by nodes and trabeculae. For each trabecula, the tensor $\langle \mathbf{C} \rangle_{micro}$ must be collinear to their z' local axis and in the case of nodes, it is proposed to use the average tensor resulting from the trabeculas belonging to the node. As a result, the tensor of elastic properties $\langle \mathbf{C} \rangle_{tb}$ will be obtained.

The whole bone is composed in its mesoscale by the trabecular bone and the cortical bone, which can be modelled using the elastic properties found in the multi-scale approach $\langle \mathbf{C} \rangle_{cb}$ and $\langle \mathbf{C} \rangle_{tb}$, respectively.

6. Conclusions

The technique use throughout this work allow us to easily model the nanoscale considering the elliptical cross section fibrils and the variation of their axis lengths. The strategy to analyse the trabecular bone, allowed us to consider the anisotropic behaviour of each trabecula and each node. Multimedia and game development software is a powerful tool for meshing complex surfaces solving a common problem in BEM procedures. This methodology is capable of handling different types of elements. Exported files contain the full geometrical information required for the evaluation of the mechanical behaviour of the hierarchical bone structure using Boundary Elements.

Acknowledgments

Disclosure statement

No potential conflict of interest was reported by the authors.

Funding

ORCID

A. F. Galvis 🆔 http://orcid.org/0000-0002-2833-2328

References

Aliabadi, M. H. (2002). *The boundary element method applications in solids and structures* (Vol. 2, Wiley Ed.). London: Author.

Amestoy, P. R., Duff, I. S., Koster, J., & L'Excellent, J.-Y. (2001). A fully asynchronous multifrontal solver using distributed dynamic scheduling. *SIAM Journal on Matrix Analysis and Applications*, *23*(1), 15–41.

Amestoy, P. R., Guermouche, A., L'Excellent, J.-Y., & Pralet, S. (2006). Hybrid scheduling for the parallel solution of linear systems. *Parallel Computing*, *32*(2), 136–156.

Barkaoui, A., Chamekh, A., Merzouki, T., Hambli, R., & Mkaddem, A. (2014). Multiscale approach including microfibril scale to assess elastic constants of cortical bone based on neural network computation and homogenization method. *International Journal For Numerical Methods In Biomedical Engineering*, *30*, 318–338.

Barkaoui, A., Tlili, B., & Vercher-Martnez, A. (2016). A multiscale modelling of bone ultrastructure elastic proprieties using finite elements simulation and neural network method. *Computer Methods and Programs in Biomedicine*, *134*, 69–78.

Benedetti, I., & Aliabadi, M. H. (2013). A three-dimensional grain boundary formulation for microstructural modeling of polycrystalline materials. *Computational Materials Science*, *67*, 249–260.

Dong, P., Pacureanu, A., Zuluaga, M. A., Olivie, C., Grimal, Q., & Peyrini, F. (2014). Quantification of the 3D morphology of the bone cell network from synchrotron micro-CT images. *Image Analysis & Stereology*, *33*, 1–10.

Fritzen, F., Hlke, T., & Schnack, E. (2009). Periodic three-dimensional mesh generation for crystalline aggregates based on Voronoi tessellation. *Computational Mechanics*, *43*, 701–713.

Galvis, A. F., Rodriguez, R. Q., & Sollero, P. (2018). Analysis of three-dimensional hexagonal and cubic polycrystals using the boundary element method. *Mechanics of Materials*, *117*, 58–72.

Galvis, A. F., Rodriguez, R. Q., Sollero, P., & Alburquerque, E. L. (2013). Multidomain formulation of BEM analysis applied to large-scale polycrystalline materials. *CMES: Computer Modeling in Engineering & Science*, *96*(2), 103–115.

Ghanbari, J., & Naghdabadi, R. (2009). Nonlinear hierarchical multiscale modeling of cortical bone considering its nanoscale microstructure. *Journal of Biomechanics*, *42*, 1560–1565.

Hamed, E., & Jasiuk, J. (2012). Elastic modeling of bone at nanostructural level. *Materials Science and Engineering*, *73*, 27–49.

He, Y., Zhan, Y., Jiang, Y., & Zhou, R. (2017). Fabrication and characterization of super-elastic TiNb alloy enhanced with antimicrobial Cu via spark plasma sintering for biomedical applications. *Journal of Materials Research*, *32*, 2510–2520.

Hill, R. (1963). Elastic properties of reinforced solids: Some theoretical principles. *Journal of Mechanics and Physics of Solids*, *11*, 357–372.

Hsu, J.-T., Wang, S.-P., Huang, H.-L., Chen, Y.-J., Wu, J., & Tsai, M.-T. (2013). The assessment of trabecular bone parameters and cortical bone strength: A comparison of micro-CT and dental cone-beam CT. *Journal of Biomechanics*, *46*, 2611–2618.

Kane, J. H. (1994). *Boundary element analysis in engineering continuum mechanics* (Prentice-Hall Ed.). New Jersey: Author.

McNally, E. A., Schwarcz, H. P., Botton, G. A., & Arsenault, A. L. (2012). A model for the ultrastructure of bone based on electron microscopy of ion-milled sections. *PLoS ONE*, *7*, e29258.

Muller, R., Campenhout, H. V., Damme, B. V., Perre, G. V. D., Dequeker, J., Hildebrand, T., & Ruegsegger, P. (1998). Morphometric analysis of human bone biopsies: A quantitative structural comparison of histological sections and micro-computed tomography. *Bone*, *23*, 59–66.

Nair, A. K., Gautieri, A., & Buehler, M. J. (2014). Role of intrafibrillar collagen mineralization in defining the compressive properties of nascent bone. *Biomacromolecules*, *15*, 24942500.

Podshivalov, L., Fischer, A., & Bar-Yoseph, P. Z. (2014). On the road to personalized medicine: Multiscale computational modeling of bone tissue. *Archives of Computational Methods in Engineering*, *21*, 399–479.

Reiser, M., Hricak, H., & Knauth, M. (2013). *Osteoporosis and bone densitometry measurements* (Vol. 1, G. Guglielmi Ed.). Berlin: Springer.

Rho, J.-Y., Kuhn-Spearing, L., & Zioupos, P. (1998). Mechanical properties and the hierarchical structure of bone. *Medical Engineering and Physics*, *20*, 92–102.

Ritchie, R. O., Buehler, M. J., & Hansma, P. (2009). Plasticity and toughness in bone. *Physics Today*, *62*(6), 41–46.

Ryan, G., Pandit, A., & Apatsidis, D. P. (2006). Fabrication methods of porous metals for use in orthopaedic applications. *Biomaterials*, *27*, 2651–2670.

Sabet, F. A., Najafi, A. R., Hamed, E., & Jasiuk, I. (2016). Modelling of bone fracture and strength at different length scales: A review. *Interface Focus*, *6*, 20150055.

Schwarcz, H. P., McNally, E. A., & Botton, G. A. (2014). Dark-field transmission electron microscopy of cortical bone reveals details of extrafibrillar crystals. *Journal of Structural Biology*, *188*, 240–248.

Shiah, Y. C., Tan, C. L., & Wang, C. Y. (2012a). Efficient computation of the Green's function and its derivatives for three-dimensional anisotropic elasticity in BEM analysis. *Engineering Analysis with Boundary Elements*, *36*, 1746–1755.

Shiah, Y. C., Tan, C. L., & Wang, C. Y. (2012b). An efficient numerical scheme for the evaluation of the fundamental solution and its derivatives in 3D generally anisotropic elasticity. *Advances in Boundary Element and Meshless Techniques XIII*, *87*(1), 190–199.

Shirazia, H. A., Ayatollahia, M. R., & Asnafib, A. (2017). To reduce the maximum stress and the stress shielding effect around a dental implant bone interface using radial functionally graded biomaterials. *Computer Methods in Biomechanics and Biomedical Engineering*, *20*, 750–759.

Sun, X. S., Tan, V. B. C., Chen, Y., Tan, L. B., Jaiman, R. K., & Tay, T. E. (2014). Stress analysis of multi-layered hollow anisotropic composite cylindrical structures using the homogenization method. *Acta Mechanica*, *225*, 1649–1672.

Tan, C. L., Shiah, Y. C., & Wang, C. Y. (2013). Boundary element elastic stress analysis of 3D generally anisotropic solids using fundamental solutions based on Fourier series. *International Journal of Solids and Structures*, *50*, 2701–2711.

Vaughan, T., McCarthyb, C., & McNamaraa, L. (2012). A three-scale fnite element investigation into the effects of tissue mineralisation and lamellar organisation in human cortical and trabecular bone. *Journal of the Mechanical Behavior of Biomedical Materials*, *12*, 50–62.

Yoon, Y. J., & Cowin, S. C. (2008). The estimated elastic constants for a single bone osteonal lamella. *Biomechanics and Modeling in Mechanobiology*, *7*, 1–11.

Zohdi, T. I., & Wriggers, P. (2005). *An introduction to computational micromechanics* (Vol. 20, T. I. Zohdi & P. Wriggers Eds.). Berlin: Springer.